Simulation and Multiobjective Optimization of an Industrial Hydrogen Plant Based on Refinery Off-Gas

P. P. Oh, G. P. Rangaiah, and Ajay K. Ray*

Department of Chemical and Environmental Engineering, National University of Singapore, 10 Kent Ridge Crescent, Singapore 119260, Singapore

A rigorous model is developed for simulating an existing industrial hydrogen plant based on refinery off-gas, which is made up of liquefied petroleum gas and off-gas from the membrane separation unit in a petroleum refinery. The presence of higher hydrocarbons in the reaction system is accounted for in the model equations for bulk gas and catalyst pellet. The reformer model is validated against three sets of industrial plant data, with good agreement. Thereafter, multiobjective optimization is performed using the nondominated sorting genetic algorithm to predict sets of Pareto-optimal operating conditions for improved performance. For a fixed feed rate of off-gas to the unit, two or three objectives, namely, maximization of product hydrogen and export steam rates and minimization of the heat duty supplied to the steam reformer, are targeted simultaneously. The optimal heat flux profile in the steam reformer is distinct from that predicted for methane feed (Oh, P. P.; Ray, A. K.; Rangaiah, G. P. *J. Chem. Eng. Jpn.* **2001**, *34* (11), 1341. The optimal results obtained are better than industrial operating data.

Introduction

Steam reforming of hydrocarbons has established itself as the most economic and preferred process for the production of hydrogen and synthesis gas. In view of the large value addition involved in the process and its high energy consumption coupled with increasing energy cost, the optimal operation of such units is of utmost concern to the industry. The choice of feedstock for steam reforming is largely determined by location, availability, and the local energy policy.[2] Common feedstocks range from natural gas to heavy naphtha. Because even the simplest of these feedstocks contains many components (natural gas contains mainly methane but also ethane, propane, butane, and other higher hydrocarbons), a multitude of chemical reactions occur in the steam reformer, making it impractical to account for all of them.

Reformation experiments carried out with hydrocarbons such as propane, butane, hexane, and benzene suggest methane to be the primary product of the reaction. Based on this observation, many published works[3−5] on steam reforming with heavier hydrocarbons assume that all hydrocarbons heavier than methane hydrocrack to methane instantaneously at the reformer inlet. As a result, the reaction system within the reformer can be reduced to that for the steam−methane reaction regardless of the feedstock used. This simplifying assumption gained wide acceptance because it was found to be satisfactory for predicting the gas composition at the reformer outlet. This is primarily because the reforming reactions are thermodynamically and not kinetically controlled. However, axial conversion profiles in an ammonia plant steam reformer[2] suggest that methanation is completed between 2 and 6 m from the entrance to the reformer, depending on the composition of the feedstock. Therefore, the assumption of instantaneous cracking cannot be valid if one wishes to model the steam reformer for nonmethane feed accurately.

In addition to the studies mentioned,[3−5] Elnashaie and Elshishini[6] provided a comprehensive review of published works in the fields of steam reforming and shift conversion kinetics, as well as steam reformer and shift converter modeling. Besides the many studies on reactor modeling, there are also a limited number of published works on the optimization of hydrogen plants. Rajesh et al.[7] optimized the performance of a side-fired steam reformer with dual objectives of minimizing the methane feed rate and maximizing the flow rate of carbon monoxide, for a fixed hydrogen production rate. Subsequently, Rajesh et al.[8] also optimized the performance of a hydrogen plant, complete with models for shift converters and steam generators, by considering simultaneous maximization of product hydrogen and export steam flow rates for a fixed methane feed rate. On the basis of the same hydrogen plant model, Oh et al.[1] obtained optimal operating conditions for a hydrogen plant, including optimal heat flux profiles in the steam reformer, by considering a third objective function—minimization of the total heat duty of the steam reformer—in addition to the two mentioned above. Considerable improvement in the objectives could be achieved by replacing the furnace gas temperature in the reformer (considered by Rajesh et al.[8]) with the heat flux profile as a decision variable. More useful information could also be gained from the addition of the third objective at no cost to computational time.

In this study, a rigorous model taking into account the presence of hydrocarbons heavier than methane and their hydrogenolysis reactions for simulating an industrial side-fired steam reformer based on refinery off-gas is developed and verified against plant data. To the best of our knowledge, this is the first published study on

* To whom correspondence should be addressed. E-mail: cheakr@nus.edu.sg. Fax: (65) 7791936.

10.1021/ie010277n CCC: $22.00
Published on Web 03/27/2002

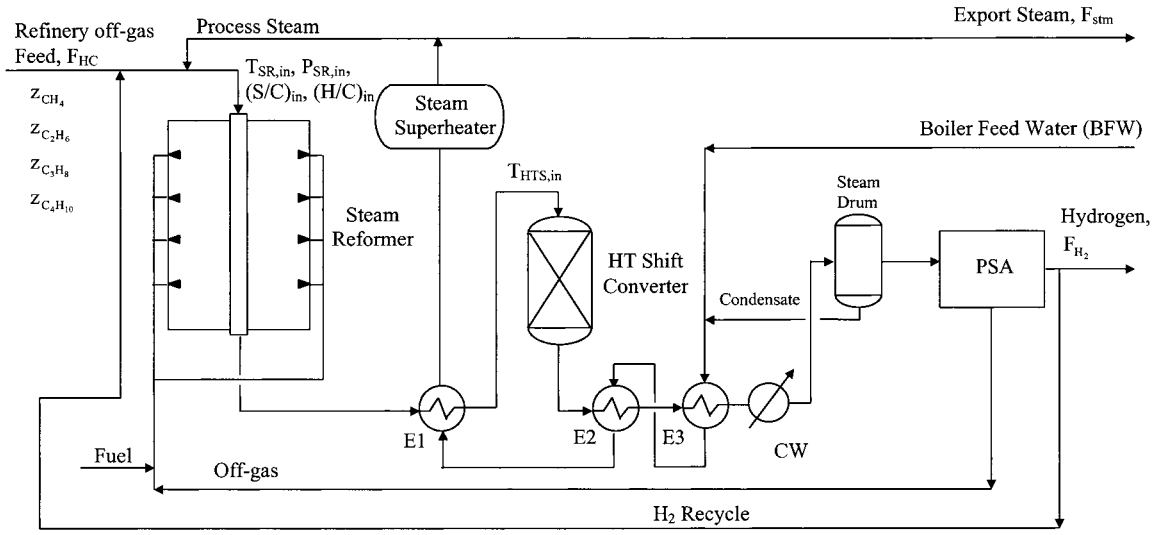

Figure 1. Simplified process flow diagram of the industrial H_2 plant using refinery off-gas.

rigorous simulation of a steam reformer based on feed heavier than methane. Thereafter, optimal operating conditions for the complete hydrogen plant using refinery off-gas as the feed are obtained by considering simultaneous maximization of product hydrogen and export steam flow rates and minimization of reformer heat duty for a fixed hydrocarbon feed rate. As in the work by Oh et al.,[1] reformer heat flux profile is considered a decision variable in optimization, thus predicting an optimal heat flux profile for each Pareto-optimal solution. The multiobjective optimization problem is solved using a nondominated sorting genetic algorithm
(GA).

Process Description

Figure 1 shows a simplified flow diagram of the industrial hydrogen unit considered in this study. The feed to the reformer furnace is comprised of refinery off-gas (assumed to contain methane, ethane, propane, and butane only), mixed with suitable quantities of recycle H_2 and steam, which are required to maintain the reformer catalyst in its active state and to prevent carbon formation, respectively. The reactions occurring in the reformer are methanation reactions (which convert hydrocarbons heavier than methane into methane) and steam−methane reforming reactions:

$$C_2H_6 + H_2 \rightleftharpoons 2CH_4 \qquad \Delta H_r = -6.44 \times 10^4 \text{ kcal/kmol} \quad (1)$$

$$C_3H_8 + 2H_2 \rightleftharpoons 3CH_4 \qquad \Delta H_r = -1.20 \times 10^5 \text{ kcal/kmol} \quad (2)$$

$$C_4H_{10} + 3H_2 \rightleftharpoons 4CH_4 \qquad \Delta H_r = -1.72 \times 10^6 \text{ kcal/kmol} \quad (3)$$

$$CH_4 + H_2O \rightleftharpoons CO + 3H_2 \qquad \Delta H_r = 2.06 \times 10^5 \text{ kcal/kmol} \quad (4)$$

$$CO + H_2O \rightleftharpoons CO_2 + H_2 \qquad \Delta H_r = -4.11 \times 10^4 \text{ kcal/kmol} \quad (5)$$

$$CH_4 + 2H_2O \rightleftharpoons CO_2 + 4H_2 \qquad \Delta H_r = 1.65 \times 10^5 \text{ kcal/kmol} \quad (6)$$

The methanation reactions (eqs 1−3) are completed in the first few meters of the reformer tubes. The two reforming reactions (eqs 4 and 6) occur mainly in the steam reformer, while thermodynamics favor the shift reaction (eq 5) in the high-temperature (HT) shift converter. (An additional low-temperature shift converter may be present in some plants to achieve additional CO conversion, but it is absent in the industrial unit modeled.) The surplus heat in the process gas at the reformer outlet is recovered (in E1) and used to generate very high pressure (VHP) steam. Part of this steam is mixed with feed, while the remainder is exported outside the unit. The shift reaction (eq 5) occurring in the HT shift converter produces additional H_2. The hot syngas leaving the shift converter is used to preheat boiler feedwater (in E2) before it is further cooled and flashed to remove entrained steam as condensate, which is recycled back to the process. The H_2-rich stream then enters a pressure-swing adsorber (PSA), which separates H_2 from off-gases. The PSA off-gas is used to supplement external fuel for combustion in the reformer furnace.

Hydrogen Plant Model

The model of the hydrogen plant developed by Rajesh et al.[8] is adapted for use in this study. They assumed pure methane feed to the unit and incorporated the kinetic rate expressions developed by Xu and Froment.[9] The heat-transfer model proposed by Singh and Saraf[4] for side-fired steam reformers and the simplified model II of Elnashaie and Elshishini[6] for intrapellet calculations were also included in the reformer model. The method of orthogonal collocation on finite elements (OCFE) was used to solve for intrapellet concentration profiles and effectiveness factors at an axial location in the reactor. The shift converter model used is similar to that of Elnashaie and Alhabdan.[10] The quantity of steam produced is found from energy balance on the heat exchangers used to recover heat from the process

gases. The steam separator was modeled as an isothermal flash of the process gas that is cooled to room temperature. The PSA unit was modeled as a "black box" with 90% hydrogen recovery and 99.5% hydrogen purity in the product, because the desired hydrogen yield and purity can be achieved by making minor modifications to adsorption/desorption cycle times to account for nominal perturbations in PSA feed composition and pressure.[11] The reader is referred to the works of Rajesh et al.[7,8] for a detailed description of the model equations.

While the above model was being adapted for this work, a programming error was uncovered in the model of the steam generation system. The error resulted in steam generation from process gas heat recovery being disproportionately large when in actual fact, the quantity of steam produced is barely sufficient to supply the internal process requirement. A shortcoming of the model of Rajesh et al.[7,8] was hence that it fails to account for steam generation based on heat recovered from flue gases exiting the furnace. This typically contributes to 60% of the total steam generation in industrial units. In this work, the quantity of steam produced by heat recovery from the process gas was found from energy balance on the waste−heat exchangers. Subsequently, total steam generation is calculated based on the assumption that this accounts for 40% of total production.

Two further modifications were made to the model of the steam reformer used by Rajesh et al.[7] First, the model was adapted for refinery off-gas feed containing ethane, propane, and butane, in addition to methane. Because the methanation reactions are completed in the steam reformer, the process gas entering subsequent process units contains methane as the only hydrocarbon. Consequently, modifications need only be made to the model of the steam reformer if the model of the entire hydrogen plant in Rajesh et al.[8] were to be adapted to an off-gas feed.

In this work, methanation reactions, along with the original steam reforming reactions, are included in the reaction system in the reformer. The heat released by methanation is incorporated in the overall energy balance. In the catalyst pellet, the heavier hydrocarbons are also considered in the formulation of the flux equations, which are solved for the effective diffusivities of all components using the simplified model II of Elnashaie and Elshishini.[6] The method of OCFE is then used to solve for intrapellet concentration profiles and effectiveness factors at an axial location in the reactor. The catalyst pellet is modeled as a slab, with two finite elements extending over $0 \le v \le 0.2$ (outer region) and $0.2 \le v \le 1.0$ (inner region). Ten orthogonal collocation points are used in the first finite element. The component fluxes are assumed to be zero at $v = 0.2$, implying that 80% of the catalyst slab (considered the second finite element) is at equilibrium.

The kinetic model developed by Xu and Froment[9] was used to model the steam reforming reactions. Suitable rate expressions and kinetic data for the hydrogenolysis of ethane, propane, and butane on the Ni/Mg_2AlO_4 catalyst employed by Xu and Froment[9] in their experiments could not be found in the literature. There exist, however, some studies on the reaction of these compounds on Ni on a variety of other supports. Kinetic rate expressions from three independent studies[12−14] of the hydrogenolysis of ethane, propane, and butane on Ni/SiO_2 were incorporated into the model, with suitable weighting factors, β_2 and β_3, on the preexponential factors in the rate constants for propane and butane, respectively; see eqs A3−A5 in appendix I. Conversion profiles of hydrocarbons heavier than methane in an industrial steam reformer[2] indicate that methanation is typically completed between 2 and 6 m from the inlet of the reformer. The actual distance for complete methanation, however, depends on the composition of the feedstock, as well as on the operating temperature. The weight on the preexponential factor for propane reaction (β_2) hastens the intrinsic rate of hydrogenolysis of propane sufficiently to ensure complete methanation within the first few meters from the reformer entrance; without it, propane was predicted in the reformer exit stream. The reaction kinetics are also of concern in the solution of the flux equations inside the catalyst pellet. The fractional weight on the preexponential factor for butane reaction (β_3) retards the intrinsic rate of hydrogenolysis of butane so as to ensure that its intrapellet mole fraction does not become negative. The application of weighting factors (β_2 and β_3) is justified in view of the incompatibility in catalyst and experimental conditions.

The adsorption equilibrium constants for ethane, propane, and butane on the Ni/Mg_2AlO_4 catalyst are also unavailable in the open literature. Therefore, they are assumed to be identical to that of methane. Because it was found that these values have an insignificant effect on the simulation results, the use of such an estimate is justified.

The second modification to the steam reformer model concerns the solution of the energy balance. Rajesh et al.[8] assumed the furnace gas temperature to be constant throughout the length of the reformer. The model equations of Singh and Saraf[4] for heat transfer from the furnace to the tubes were solved together with the energy balance to determine the heat flux at any axial location. In this work, for the purpose of predicting an optimal heat flux profile, the reformer axial heat flux profile was expressed as a quadratic function of the tube length. The heat-transfer equations (eqs A21−A23 in appendix I) were then solved in conjunction with the heat flux and process gas temperature at any axial location. The reformer model equations and sources of data are summarized in appendix I. The catalyst data used in this study are available in Elnashaie and Elshishini.[6]

Formulation of the Optimization Problem

For a fixed feed rate of hydrocarbons to the unit, F_{HC}, the profitability of operating a hydrogen plant will depend on the revenue generated from the sale of hydrogen and steam, as well as the outlay on fuel. If accurate and generalized cost values could be obtained, these factors could be combined into a single parameter, the profitability function, to be minimized during optimization. However, the unavailability of such data implies that a multiobjective optimization is necessary in order to predict optimal operating conditions for hydrogen plant operation. Moreover, required hydrogen and steam flow rates are plant specific.

Optimization Problem for Two Objectives. The simultaneous maximization of the flow rates of product hydrogen, F_{H_2}, and export steam, F_{stm}, are first considered in multiobjective optimization because these are the primary factors that dictate the economics of

hydrogen plant operation. The optimization problem is formulated as

$$\text{maximize} \qquad J_1 = F_{H_2} \tag{7}$$

$$J_2 = F_{stm} \tag{8}$$

$$\text{subject to} \qquad T_{w,max} \le 1200 \text{ K} \tag{9}$$

$$\left[\frac{y_{H_2O}}{y_{H_2}}\right]_{HTS} \ge 0.3 \tag{10}$$

$$Q_{Ei} \le 1.2Q_{Ei\,max} \qquad i = 1-3 \tag{11}$$

$$F \le 1.2F_{max} \tag{12}$$

At operating temperatures exceeding 1200 K, the reformer tube metal creeps under thermal stress, resulting in rupture. Equation 9 is used in order to prolong the life of the tubes. Equation 10 is based on thermodynamic considerations, to prevent the reversal of the shift reaction (eq 5) within the shift converter. The duties of the heat exchangers (eq 11) and the total feed rate to the unit (eq 12) must conform to design margins.

The reformer axial (outer surface) heat flux profile, q, is expressed as a function of the tube length, z. As compared to a top-fired furnace design, the side-fired system has many burners at varying heights to provide greater flexibility in controlling the heat input to the reformer. The typical heat flux profile in an industrial reformer is parabolic with a dominant peak near the entrance.[15] To allow more scope in the selection of the optimal heat flux profiles, two quadratic functions are used to model the sections of the tube preceding and following the point of maximum heat flux, z^*.

For $z \le z^*$

$$q = A + B\left(\frac{z}{z^*}\right) + C\left(\frac{z}{z^*}\right)^2 \tag{13a}$$

For $z > z^*$

$$q = A + B + C + D\left(\frac{z - z^*}{L}\right) + E\left(\frac{z - z^*}{L}\right)^2 \tag{13b}$$

where L is the total tube length. Thus, the coefficients $A-E$ and z^* in the above equations specify the heat flux profile.

The optimization problem has 11 decision variables. Ten of them (eq 14a−j) fully define the operation of the steam reformer, while the remaining one (eq 14k) specifies the inlet temperature to the adiabatic HT shift converter. The following bounds are used for the decision variables:

$$725 \le T_{SR,in} \le 900 \text{ K} \tag{14a}$$

$$2450 \le P_{SR,in} \le 2950 \text{ kPa} \tag{14b}$$

$$2.0 \le (S/C)_{in} \le 6.0 \tag{14c}$$

$$0.0 \le (H/C)_{in} \le 0.5 \tag{14d}$$

$$20\,000 \text{ kcal m}^{-2} \text{ h}^{-1} \le A \le 80\,000 \text{ kcal m}^{-2} \text{ h}^{-1} \tag{14e}$$

$$0 \le B \le 60\,000 \text{ kcal m}^{-2} \text{ h}^{-1} \tag{14f}$$

$$-30\,000 \text{ kcal m}^{-2} \text{ h}^{-1} \le C \le 0 \tag{14g}$$

$$-60\,000 \text{ kcal m}^{-2} \text{ h}^{-1} \le D \le 0 \tag{14h}$$

$$-60\,000 \text{ kcal m}^{-2} \text{ h}^{-1} \le E \le 30\,000 \text{ kcal m}^{-2} \text{ h}^{-1} \tag{14i}$$

$$0.5 \le z^* \le 2.0 \tag{14j}$$

$$570 \le T_{HTS,in} \le 730 \text{ K} \tag{14k}$$

The limits on $T_{SR,in}$ are dependent on thermodynamic considerations to prevent gum formation in the catalyst and on the maximum heat typically transferred from the furnace gas in the convection section of the reforming furnace to the feed, respectively. The bounds on $P_{SR,in}$ are based on the pressure required of product hydrogen and on the supply pressure of the feed. A very low value of $(S/C)_{in}$ may cause coking and shift-reaction problems and even result in high methane leakage from the reformer. However, higher $(S/C)_{in}$ increases the mass flow through the plant and thus the size and cost of the equipment. The bounds on $(S/C)_{in}$ are chosen based on these considerations. The upper limit on $(H/C)_{in}$ is selected to avoid redundant hydrogen recycle back to the reformer. Bounds on $T_{HTS,in}$ are based on the normal operating range in industrial units.

The high alloy reformer tubes contribute significantly to the reformer costs.[15] Their reliability is also important because tube failures would result in downtime and loss of production. These tubes are, however, adversely affected by the thermal stresses caused by the temperature gradient over the tube wall, and this limits the maximum allowable heat flux for a given operating temperature and tube inner diameter. The maximum heat flux conventionally applied in industrial units varies from 95 to 110 Mcal/(h·m^2).[16] To be conservative, limits on q were fixed between 20 and 80 Mcal/(h·m^2). The bounds on A correspond to those on q, while those on $B-E$ allow maximum flexibility in selecting an optimum heat flux profile which satisfies the specified bounds on q while conforming to the constraint of zero gradient at the maximum point, z^*. The range for z^* (eq 14j) is based on typical industrial profiles.[15]

Because the optimization program developed by our group is for minimization, maximization of F_{H_2} and F_{stm} was replaced by the minimization of their reciprocals. In addition, the performance constraints (eqs 9−12) were incorporated into the objective functions as penalty functions. The objective functions may now be written as

$$I_1 = \frac{10^3}{F_{H_2}} + 10^4\sum_{i=1}^{6} f_i \tag{15}$$

$$I_2 = \frac{10^3}{F_{stm}} + 10^4\sum_{i=1}^{6} f_i \tag{16}$$

where

$$f_1 = (T_{w,max} - 1200) + |(T_{w,max} - 1200)| \tag{17a}$$

$$f_2 = \left[0.3 - \frac{y_{H_2O}}{y_{H_2}}\right] + \left|\left[0.3 - \frac{y_{H_2O}}{y_{H_2}}\right]\right| \quad (17b)$$

$$f_3 = (Q_{E1} - 1.2Q_{E1\,max}) + |(Q_{E1} - 1.2Q_{E1\,max})| \quad (17c)$$

$$f_4 = (Q_{E2} - 1.2Q_{E2\,max}) + |(Q_{E2} - 1.2Q_{E2\,max})| \quad (17d)$$

$$f_5 = (Q_{E3} - 1.2Q_{E3\,max}) + |(Q_{E3} - 1.2Q_{E3\,max})| \quad (17e)$$

$$f_6 = (F - 1.2F_{max}) + |(F - 1.2F_{max})| \quad (17f)$$

The weighting factors used in eqs 15 and 16 give a similar range in magnitude of values for the objective functions to avoid numerical problems.

Optimization Problem for Three Objectives. The optimization problem (consisting of eqs 13−17) is later extended to three objectives: simultaneous maximization of F_{H_2} and F_{stm} and minimization of the consumption of furnace fuel. The inclusion of the third objective, however, poses a difficulty owing to the manner in which the requirement of furnace fuel is determined in the model. The total heat duty required by the reformer, Q_{SR}, is found by integrating the heat flux on the reformer tubes along the tube length. A fraction of Q_{SR} is supplied by the PSA off-gas, with the remainder made up by natural gas and/or refinery fuel gas which constitute furnace fuel, Q_{fuel}. Q_{fuel} is found from the difference between Q_{SR} and the heating value of the PSA off-gas. However, the heating value of the off-gas is a function of its flow rate and composition, both of which are governed by the methane leakage from the reformer. Consequently, a high methane leakage from the reformer would increase the heating value of the PSA off-gas, enabling this stream to supply a larger fraction of Q_{SR}, hence decreasing the consumption of furnace fuel. However, a high methane leakage also implies poorer conversion in the reformer and shift converter, which leads to adverse effects on hydrogen and steam production. In other words, if minimization of furnace fuel consumption were considered as an objective, optimization would predict some operating scenarios, which artificially lower fuel consumption by perpetrating a high methane leakage, at the expense of hydrogen and steam production. Therefore, minimization of Q_{SR} is considered as the third objective to yield energy-efficient operating scenarios, in addition to the first two objectives in eqs 7 and 8.

$$\text{minimize} \qquad J_3 = Q_{SR} \quad (18)$$

Other than the performance constraints defined in eqs 9−12, an additional constraint on the fraction of the total reformer duty, Q_{SR}, supplied by furnace fuel, Q_{fuel}, is necessary

$$Q_{fuel}/Q_{SR} \geq 0.55 \quad (19)$$

The value of the constraint (eq 19) is based on typical industrial values.[16] This constraint is essential in order to avoid optimal operating scenarios with negative or low values of Q_{fuel}/Q_{SR}. Negative values of Q_{fuel}/Q_{SR} are encountered when a high methane leakage from the reformer raises the heating duty of the PSA off-gas to the extent that it is more than able to supply Q_{SR}. In these cases, Q_{fuel}, found from the difference between Q_{SR} and the duty supplied by the off-gas, will be negative. Such operating scenarios, along with those with positive but low Q_{fuel}/Q_{SR}, are regarded as "optimal" because they are associated with a minimal Q_{SR}, thus satisfying at least one objective.

Table 1. Design Data and Other Parameters for Steam Reformer and HT Shift Converter[a]

quantity	value
Steam Reformer	
heated length of reformer tubes, L	11.55 m
inside diameter of reformer tubes, d_i	0.102 m
outside diameter of reformer tubes, d_o	0.136 m
no. of tubes	84
catalyst bed void fraction, ϵ_b	0.4[b]
tube thermal conductivity[19]	$10.738 + 0.0242T_w$
HT Shift Converter	
reactor length	2.4 m
reactor diameter	2.4 m

[a] All data are for the industrial plant modeled in this study. [b] The value of ϵ_b was obtained by trial and error to match the reformer exit pressure.

The performance constraints (eqs 9−12 and 19) were incorporated into the objective functions as penalty functions. In addition to the objective functions in eqs 15 and 16, the third objective function is written as

$$I_3 = \frac{Q_{SR}}{10^2} + 10^4 \sum_{i=1}^{7} f_i \quad (20)$$

where f_1−f_6 are defined in eq 17a−f and

$$f_7 = \left[\frac{Q_{fuel}}{Q_{SR}} - 0.55\right] - \left|\left[\frac{Q_{fuel}}{Q_{SR}} - 0.55\right]\right| \quad (21)$$

The optimization problems for both two and three objective functions are solved using the nondominated sorting GA (NGSA), which is found to be suitable for multiobjective problems. Details on NSGA can be found in works by Srinivas and Deb[17] and Bhaskar et al.[18] The NSGA parameters used in this work, except for the generation number, can be found in the work by Rajesh et al.[7]

Results and Discussion

Simulation of the Reformer Based on Refinery Off-Gas Feed. Design data and other parameters for steam reformer and shift converter in the industrial hydrogen plant used in this work can be found in Table 1. The model developed for the reformer was implemented and solved on the SGI Origin 2000 supercomputer using the mathematical routines DIVPAG (for integration of stiff ordinary differential equations) and DNEQNF (for solving the set of algebraic collocation equations) available in IMSL. The CPU time for simulating the hydrogen plant using an off-gas feed is 52 s, 10 times more than that needed to simulate a hydrogen plant based on a methane feed. This is mainly attributed to the iterations necessary to yield good initial estimates for the successful solution of intrapellet collocation equations to find intrapellet concentrations. In the case of a methane feed, initial estimates were obtained from published intrapellet concentration profiles.[6] The same, however, could not be found for a feed containing higher hydrocarbons. Initial estimates for this case were hence obtained starting from intrapellet concentration profiles for a methane feed, gradually incrementing the

Table 2. Comparison between Plant Data and Simulation Results[a]

variable	case 1	case 2	case 3
Reformer Inlet Conditions			
$T_{SR,in}$ (K)	728.9	753.8	759.2
$P_{SR,in}$ (kPa)	1979.8	1970.6	2116.5
$(S/C)_{in}$	3.94	3.75	4.25
$(H/C)_{in}$	0.329	0.450	0.336
F (kmol/h)	1224.8	1227.8	1060.9
$F_{HC,in}$	110.25	114.29	88.22
Refinery Off-Gas Composition, mol %			
z_{CH_4}	20.11	24.39	20.74
$z_{C_2H_6}$	36.94	35.35	35.35
$z_{C_3H_8}$	28.63	24.29	26.71
$z_{C_4H_{10}}$	14.25	15.88	17.20
T_g[b] (K)	1437.0	1433.0	1396.0

	case 1		case 2		case 3	
	simul.	actual	simul.	actual	simul.	actual
Reformer Exit Conditions						
T_{SR} (K)	1101	1101	1102	1102	1103	1103
P_{SR} (kPa)	1695	1712	1792	1732	1737	1735
F_{SR} (kmol/h)	1697.7	-	1696.1	-	1454.0	-
Process Gas Composition, mol % (Wet Basis)						
y_{CH_4}	1.47	1.07	1.27	1.16	1.76	1.56
y_{H_2O}	40.26	40.51	42.45	44.41	38.64	39.43
y_{CO}	7.52	6.13	6.95	7.93	7.75	7.92
y_{CO_2}	6.40	9.46	6.42	6.09	6.09	6.70
y_{H_2}	44.34	42.83	42.90	44.41	45.77	44.39

[a] There is no CO_2 or CO in the actual plant feed; hence, $(D/C)_{in} = (M/C)_{in} = 0$. However, to prevent division by zero during intrapellet mole fraction calculation, $(D/C)_{in} = 10^{-5}$ is used in the program. [b] Obtained by trial and error to match reported results.

amount of higher hydrocarbons in the feed and solving collocation equations for each increment until the actual feed composition is reached. Because the good initial guess is highly sensitive to feed composition, very small increments were used. Longer CPU time is also partly caused by an increase in the number of components (from 5 to 8) and reactions (from 3 to 6) leading to a corresponding increase in the number of ODEs (from 5 to 8) and algebraic intrapellet equations (from 5M to 8M, where M is the number of internal collocation points) to be solved.

From the preliminary trials on simulating the hydrogen plant with an off-gas feed, $\beta_2 = 1.9 \times 10^7$ and $\beta_3 = 10^{-4}$ were found to be suitable to ensure conversion of propane and butane in the first several meters of the tube length[2] and to avoid numerical problems. Although this is satisfactory for this study, it also indicates the need for basic kinetic data on methanation of hydrocarbons on the catalysts used in industrial steam reformers, for a more accurate modeling. With these values of β_2 and β_3, the model was tested for the three cases of plant data in Table 2. The paramount factor in determining methane conversion in the reformer is the process gas temperature at the reformer exit. For a fixed feed temperature, the exit temperature is dependent on the heat transferred from furnace gases to tubes. Hence, the heat flux profile, according to eq 13, can be adjusted to achieve the desired reformer exit temperature. This, however, poses a difficulty owing to the many variables involved in defining the profile (eq 13). To simplify, a constant furnace gas temperature, T_g, in the radiation section of the furnace is assumed, and the model equations of Singh and Saraf[4] are solved to compute the tube wall and process gas temperature at any axial location in the reformer. This is similar to the approach adopted by Rajesh et al.[7,8] In this way, T_g can be used as a fitting parameter to match the exit temperature of the process gas. For each case, a different T_g was found. Although all of the cases considered are for the same industrial unit, different values for T_g are expected because the fuel supplied to the furnace is varied in practice to satisfy the energy required by the reactions taking place within the reformer tubes, which is, in turn, a function of the flow rate and composition of the feedstock. Accordingly, the tuned values of T_g were found to be related to the heat duty supplied to the reformer furnace. The latter quantity can be determined from measured flow rates and heating values of the PSA off-gas and furnace fuel gas and can be used to estimate T_g for simulating different industrial cases.

When the reformer exit conditions obtained from simulation are compared with the three sets of industrial operating data (Table 2), a good match is observed, thus confirming the validity and robustness of the model developed. Figure 2 shows the axial conversion, temperature, pressure, and effectiveness factor profiles obtained from simulation of case 2 (Table 2). It can be observed from the conversion profiles that hydrogenolysis of higher hydrocarbons is completed within the first 6 m of the reformer tubes, consistent with published reports.[2] In addition, the outer tube wall temperature, $T_{w,o}$, reaches a maximum of 1200 K, consistent with the practical constraint given in eq 9. The effectiveness factor for reaction 5 shows a discontinuity owing to the reversal in the direction of the reaction at the surface of the catalyst. The intrinsic rate passes through zero at that point, resulting in the spike in effectiveness factor values and the change in sign. This phenomenon was also observed for the case of the methane feed[6,7] though there are some differences in the temperature and axial position at which the spike occurs. The latter is controlled by the temperature, pressure, and composition of the process gas, which explains the differences observed.

Multiobjective Optimization. An inherent conflict is often present between two objective functions involved in multiobjective optimization when they are influenced in opposite directions by changes in some of the decision variables. When this happens, an improvement in one objective is accompanied by deterioration in the other. As a result, multiple optimal solutions (known as a Pareto set) are be encountered. Each of these Pareto-optimal solutions is superior to another in terms of one or more objectives but inferior in terms of others. Each of these optimal solutions is associated with one set of decision variables.

While optimization was being performed, it was found that numerical solution of the reformer model equations could not be obtained for some combinations of decision variables. Hence, the range for $(S/C)_{in}$ had to be restricted based on a given inlet temperature and $(H/C)_{in}$ to ensure convergence when solving the intrapellet flux equations in the reformer model. Figure 3 shows the domain which defines the working bounds for $(S/C)_{in}$. These bounds were used in place of those defined in eq 14c when mapping the value of $(S/C)_{in}$ in the search for optimal solutions. An adaptation was made to NSGA to allow the mapping limits for $(S/C)_{in}$ to be dependent on the inlet temperature and $(H/C)_{in}$. Such a modification was also necessary in earlier optimization work on a hydrogen plant based on methane as the only hydrocarbon.[1,7,8] However, the working domain for $(S/C)_{in}$ was different in that case.

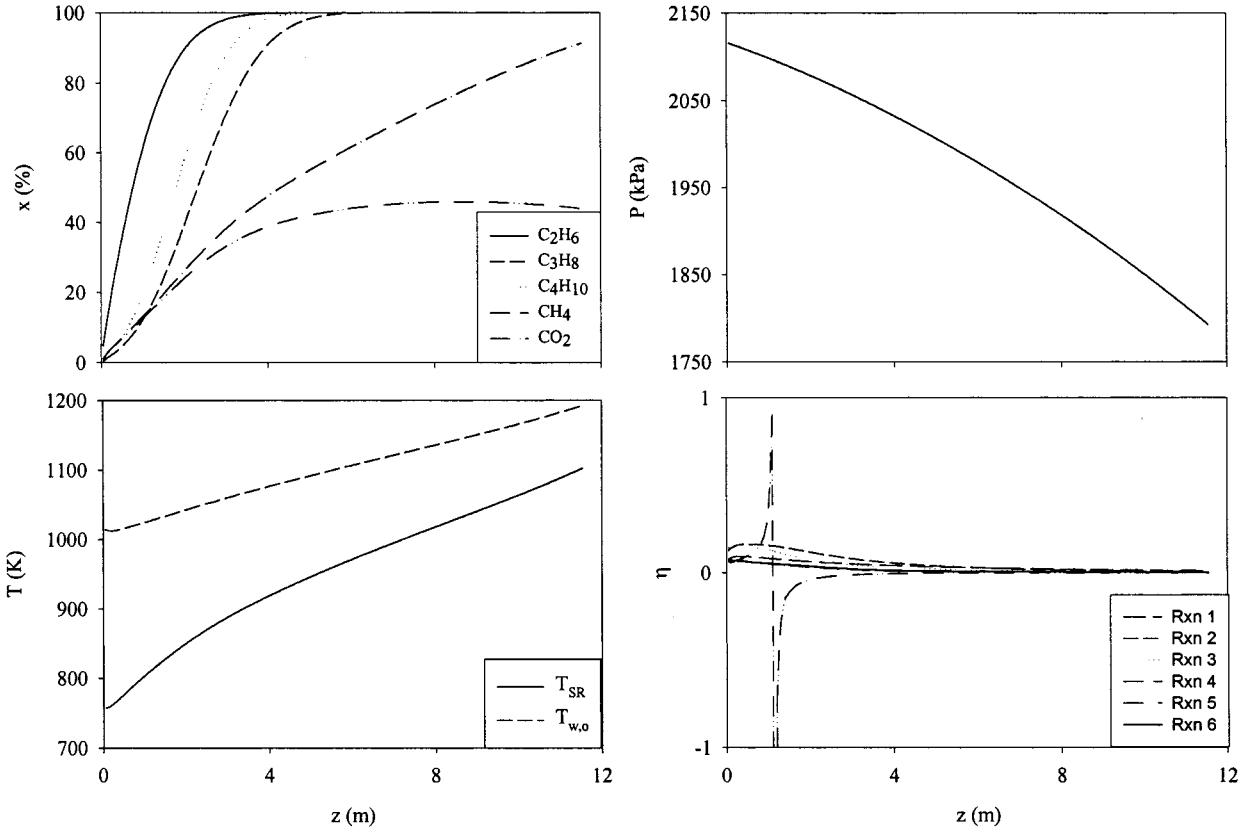

Figure 2. Steam reformer axial profiles obtained from simulation.

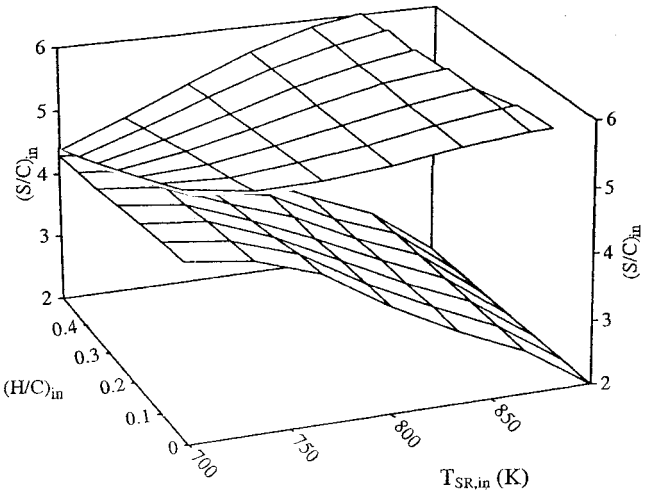

Figure 3. Lower and upper bounds of domain of $(S/C)_{in}$ for a choice of $T_{SR,in}$ and $(H/C)_{in}$.

Many chromosomes created during the search were found to violate the allowed range of 20−80 Mcal/(h·m^2) for q. This is attributable to the wide ranges allowed for variables $B-E$ (eq 14f−i). Therefore, for efficient optimization, the limits for $B-E$ were restricted based on the values of other decision variables.

$$0 \le B \le (80\,000 - A) \text{ kcal m}^{-2}\text{ h}^{-1} \quad (22a)$$

$$-0.5B \le C \le 0 \text{ kcal m}^{-2}\text{ h}^{-1} \quad (22b)$$

$$20\,000 - A - B - C \le D \le 0 \text{ kcal m}^{-2}\text{ h}^{-1} \quad (22c)$$

$$20\,000 - A - B - C - D \le E \le -0.5D \text{ kcal m}^{-2}\text{ h}^{-1} \quad (22d)$$

Similar to the case of $(S/C)_{in}$, these new bounds (eq 22a−d) were employed in place of those defined in eq 14f−i.

Optimization for Two Objectives. Optimization was performed based on the hydrocarbon flow rate and composition as per case 1 of plant data (Table 2). Figure 4a shows the optimal solutions (Pareto set) obtained from optimization with two objectives (eqs 15 and 16) after 100 generations with 50 chromosomes. The decision variables associated with the chromosomes on the Pareto set of Figure 4a are shown in Figure 4b−h. Table 3 lists the operating parameters corresponding to three selected chromosomes, F−H, on the Pareto set. To understand and explain the variation of decision variables in Figure 4, the effect of an increase in each decision variable on the objective functions is summarized in Table 4.

The endothermic reforming reactions (eqs 4 and 6) are favored at high temperatures. As such, one would expect $T_{SR,in}$ to be near its upper bound, as was observed in the case of the methane feed.[8] However, the optimized values of $T_{SR,in}$ (Figure 4b) are approximately 767 K, which is nearer to its lower bound (eq 14a). This is attributed to the methanation of heavier hydrocarbons in the initial part of the reformer tube. The release of exothermic heat of methanation reactions raises the temperature of the process gas and, consequently, the tube wall temperature. For a fixed refinery gas flow rate and composition, the extent of methanation reactions and heat release is fixed. In such a case, $T_{SR,in}$ has to be decreased to satisfy the upper bound on tube wall temperature, $T_{w,max}$ (eq 9). Because the methanation reactions (eqs 1−3) are completed within the first few meters in the reformer tube, they have no effect on the reformer output or the objectives. For this reason, other than for $T_{SR,in}$ and the heat flux profile (discussed later),

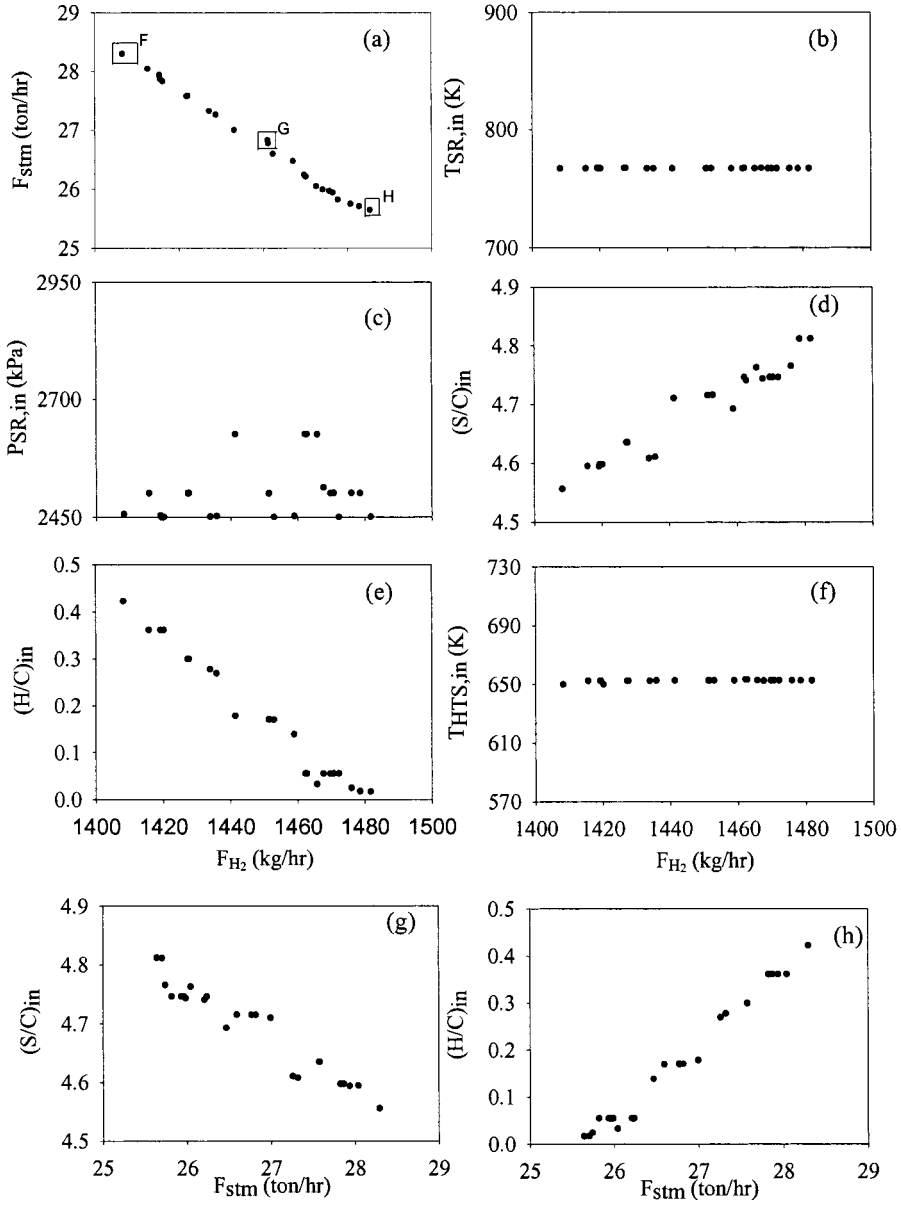

Figure 4. (a) Pareto set for two objectives obtained after 100 generations with 50 chromosomes. (b−g) Decision variables corresponding to the Pareto set in part a. $(S/C)_{in}$ and $(H/C)_{in}$ are plotted against F_{H_2} in parts d and e and against F_{stm} in parts g and h.

Table 3. Operating Parameters for Selected Chromosomes of the Pareto Sets in Figures 4 and 6[a]

	Selected Chromosomes from Figure 4 for Two Objectives			Selected Chromosomes from Figure 6 for Three Objectives		
parameter	F	G	H	7	12	17
$T_{SR,in}$ (K)	767.0	767.0	767.0	801.1	801.1	801.1
$P_{SR,in}$ (kPa)	2455.9	2500.7	2450.8	2584.2	2584.2	2582.0
$(H/C)_{in}$	0.422	0.171	0.017	0.158	0.158	0.280
$(S/C)_{in}$	4.56	4.72	4.81	4.32	4.32	4.91
$T_{HTS,in}$ (K)	650.1	652.6	652.6	644.3	644.3	600.8
F_{H_2} (kg/h)	1408.3	1451.5	1481.8	1316.0	1354.7	1406.0
F_{stm} (tons/h)	28.3	26.8	25.6	23.2	24.4	26.3
Q_{SR} (Gcal/h)	45.2	45.3	45.3	38.8	40.3	43.2
$Q_{ext\ fuel}$ (Gcal/h)	33.2	34.4	35.1	24.7	27.1	31.2
$Q_{ext\ fuel}/Q_{SR}$ (%)	73.5	75.9	77.5	63.7	67.2	72.2

[a] For case 1 of plant data (Table 2): F_{H_2} = 1342.8 kg/h, F_{stm} = 26.0 tons/h, Q_{SR} = 43.2 Gcal/h.

these reactions are ignored when considering the effect of other decision variables on the objectives.

The reforming reactions (eqs 4 and 6) are enhanced by lower pressures, while the shift conversion reaction

Table 4. Effect of an Increase in Decision Variables on the Objective Functions

	effect of increase in				
objective function	$T_{SR,in}$	$P_{SR,in}$	$(H/C)_{in}$	$(S/C)_{in}$	$T_{HTS,in}$
F_{H_2}	↑	↓	↓	↑	↓
F_{stm}	↑	↑ or ↓	↑	↓	↓
Q_{SR}	↑	↓	↓	↑	no effect

is unaffected by pressure. Hence, lower pressures lead to higher methane conversion and increased hydrogen production. The effect of pressure on steam generation is more complicated. Steam generation is a function of the energy recoverable from the process gas streams exiting the reformer (Q_{E1}) and shift converter (Q_{E2}). With a greater extent of heat recovery, more steam can be generated. For a fixed $T_{SR,in}$, feed composition, and reformer duty, Q_{SR}, the total heat input into the reformer is fixed. As such, at lower pressures, a greater fraction of the total heat input into the reformer will be consumed for the endothermic reforming reactions in the reformer, leaving a smaller amount to be recov

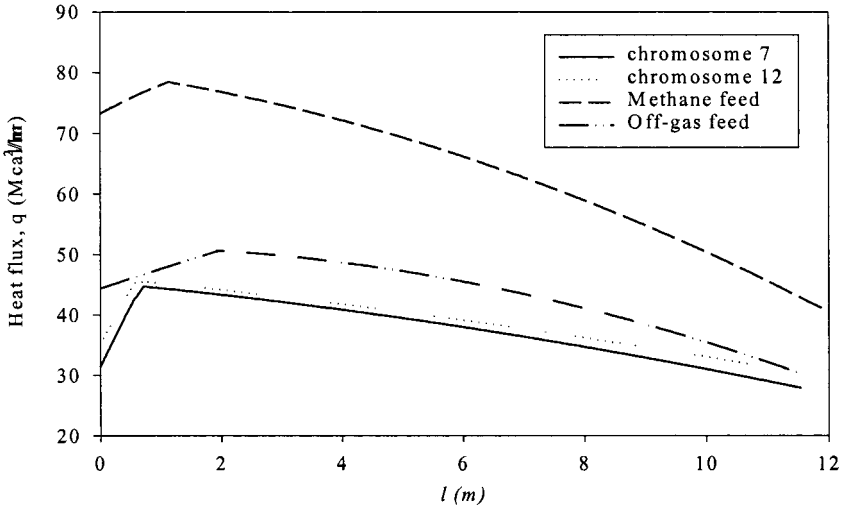

Figure 5. Optimal heat flux profiles on the reformer tubes for the Pareto set of Figure 4a (two objectives with off-gas feed) and for selected chromosomes of the Pareto set of Figure 6 (three objectives) compared with that for the case when methane is the only hydrocarbon in the feed.[1] The optimal heat flux profile for two objectives with off-gas feed is the same for all chromosomes.

ered in Q_{E1} for steam generation. On the other hand, lower pressures also result in one reforming reaction (eq 4) occurring to a higher extent than the other (eq 6), producing relatively more CO and less CO_2. This leads to a greater extent of shift conversion (eq 5) in the HT shift converter and increased heat recovery in Q_{E2}. Hence, lower pressures decrease heat recovery in Q_{E1} while increasing that in Q_{E2}. Because the steam generation is a function of the sum of these, the effect of $P_{SR,in}$ on steam generation will depend on the operating conditions (see Table 4). The ambivalent effect of $P_{SR,in}$ on steam generation was observed by varying the value of only this variable with all others fixed corresponding to a few different chromosomes. The optimal values of $P_{SR,in}$ fall nearer to the lower limit (Figure 4c), consistent with increased hydrogen production. However, some scatter is observed because of its vacillating effect on steam generation.

An increase in $(S/C)_{in}$ promotes the reforming reactions, thus increasing methane conversion and hydrogen production (Figure 4d). However, an increase in $(S/C)_{in}$ also promotes one reforming reaction (eq 6) more than the other (eq 4), generating more CO_2 and less CO in the reformer outlet, resulting in decreased conversion in the shift converters and reduced steam generation (Figure 4g). An increase in $(H/C)_{in}$ inhibits the reforming reactions, thus reducing methane conversion and hydrogen production (Figure 4e). At the same time, it inhibits one reforming reaction (eq 6) more than the other (eq 4), leading to more CO and less CO_2 in the reformer outlet, promoting increased exothermic reaction in the shift converters and increased steam generation (Figure 4h). Hence, both $(S/C)_{in}$ and $(H/C)_{in}$ have conflicting effects on F_{H_2} and F_{stm} (Table 4). Because the exothermic reactions are favored at lower temperatures, the optimized solutions predict operation at the lowest $T_{HTS,in}$ (Figure 4f) possible while satisfying the constraint (eq 12) on the heat load, Q_{E1}, on the waste−heat exchanger at the reformer outlet.

Values of decision variables $A-E$ and z^* (which define the heat flux profile according to eq 13) are almost the same for all of the chromosomes of the Pareto set of Figure 4a, indicating that one optimum heat flux profile (shown in Figure 5) is representative of all of the chromosomes in the Pareto set. This optimal heat flux profile is in contrast to the one obtained when methane was assumed to be the only hydrocarbon in the feed[1] (Figure 5). Note that the two optimization cases are for different industrial units which operate on different feed rates, and so the required furnace heat duty will be different. Hence, only the shapes, and not the numerical values, of the heat flux profiles in Figure 5 should be compared. In the case of methane feed, optimization predicts the maximum allowable heat flux in the initial part of the reformer tube where most of the reaction takes place. Further down the tube, the heat flux diminishes rapidly as conversion increases and the reactants are used up. In the case of off-gas, however, the exothermic methanation reactions will supply a large fraction of the heat required by the reforming reactions in the initial part of the tube, thus requiring a smaller supply of additional heat duty from the furnace. As the heavier hydrocarbons are depleted, less heat will be released from their methanation, and more heat duty will be required from the furnace. Beyond the initial part, the amount of reforming reactions taking place dwindles as methane is converted, and again, less furnace heat duty needs to be supplied. However, because methane is constantly produced by the methanation reactions a few meters from the tube inlet, the heat flux should diminish more slowly following the maximum compared with the methane case. The optimal heat flux profile in Figure 5 confirms this analysis by exhibiting a low entry heat flux, which peaks at about 2 m, before diminishing gradually. The distinct difference between the profiles obtained indicates that the assumption of instantaneous methanation adopted by several researchers[3−5] is not valid when we wish to predict the optimal heat flux profile.

The objectives associated with the industrial operating case 1 of Table 2, upon which the optimization study is based, are listed in the footnote of Table 3. Optimal operation predicts up to 10% increase in hydrogen production and/or steam generation over the industrial operating point. However, the furnace duty, Q_{SR}, associated with the optimal solutions is higher than case 1 of plant data. Hence, the cost of furnace fuel and the value of hydrogen and steam will determine whether the "optimal" solutions are indeed economically advantageous. In the absence of such cost data (which are site-

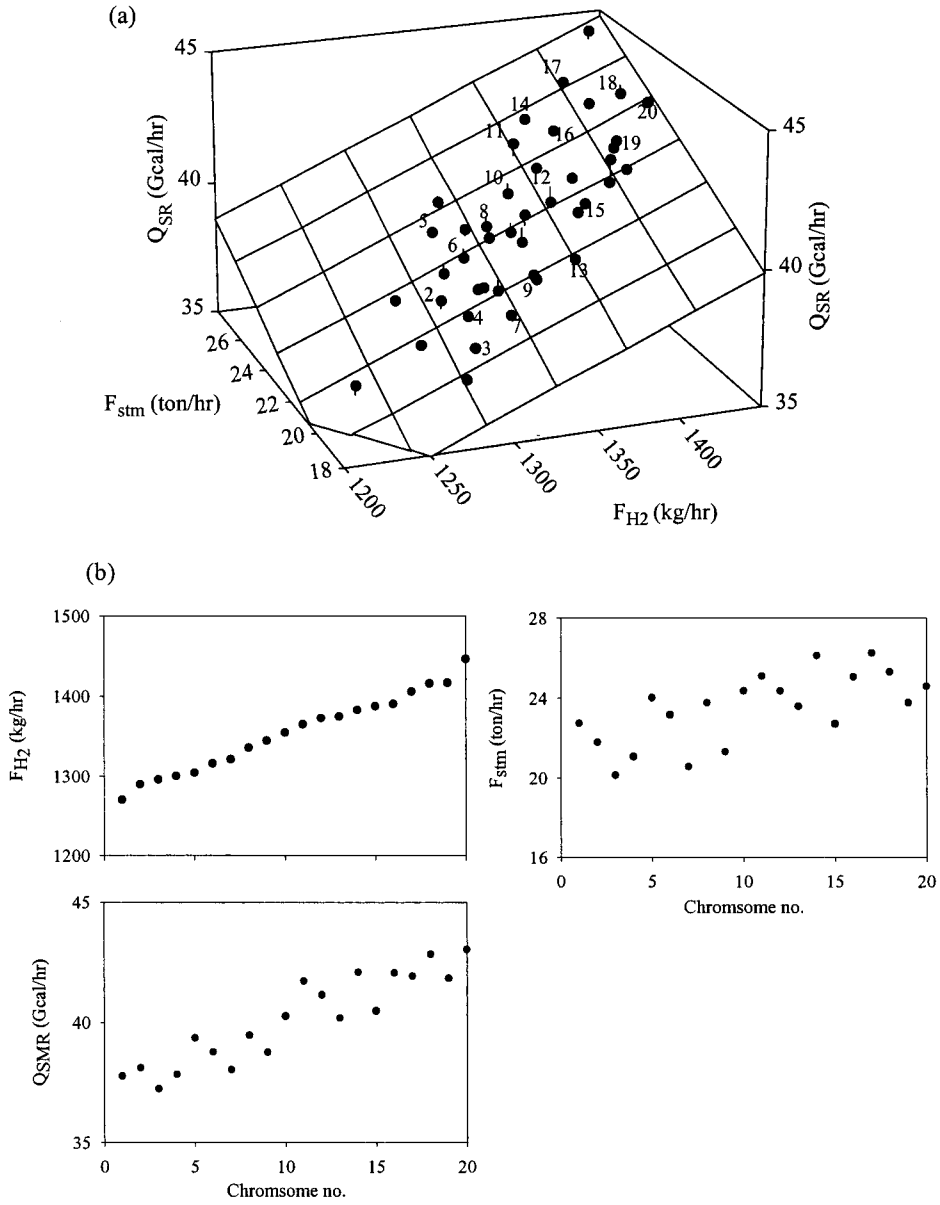

Figure 6. Pareto-optimal set for three objectives after 100 generations with 50 chromosomes. (a) Points represent chromosomes, while the wire frame represents the best-fit plane. (b) Objectives are plotted against the number of 20 selected chromosomes.

specific), it is only logical to compare scenarios with similar reformer duties, as will be done in the next section.

Optimization for Three Objectives. As in the case of two objectives, optimization was performed based on the hydrocarbon flow rate of case 1 (Table 2). Figure 6a shows, in three dimensions, the Pareto set of optimal solutions obtained from triple objective optimization (eqs 15, 16, and 20). To improve clarity, 20 chromosomes are selected from the overall set and their objective values are plotted in Figure 6b. It is observed from these plots that none of these chromosomes is superior to another in terms of all three objectives. For example, chromosome 2 is superior to chromosome 1 in terms of increased hydrogen but inferior in terms of decreased steam generation and higher reformer heat duty. Hence, neither chromosome is dominant over the other, and they are both equally good. The decision variables associated with 20 chromosomes on the Pareto set are shown in Figure 7.

The optimized solutions suggest plant operation at $T_{SR,in}$ of about 801 K and at the lowest $T_{HTS,in}$ (Figure 7c) possible while satisfying the constraint on Q_{E1} (eq 12). Significant scatter is observed in $P_{SR,in}$ (Figure 7d). These observations are consistent with those for two objectives. On the other hand, the distinct trends exhibited by $(S/C)_{in}$ and $(H/C)_{in}$ with increasing F_{H_2} and F_{stm} for two objectives (Figure 4d,e,g,h) are not observed here. Instead, $(S/C)_{in}$ (Figure 7a,e) takes one of two distinct optimal values while $(H/C)_{in}$ (Figure 7b,f) is scattered between 0 and 0.3. This conflict is best explained by considering chromosomes 7 and 12 (shown in Table 3), which share identical values of $(S/C)_{in}$ and $(H/C)_{in}$, as well as $T_{SR,in}$, $P_{SR,in}$, and $T_{HTS,in}$, and yet F_{H_2} and F_{stm} are higher in the case of chromosome 12. The difference between the two chromosomes can be attributed to their different reformer heat flux profiles. As can be observed in Figure 5, the optimal heat flux profiles are similar in shape to those for two objectives (Figure 5). However, the heat flux for chromosome 12 is nearly 10% higher than that for chromosome 7 at the reformer inlet. From the entrance, the profile for chromosome 12 increases at a rate comparable to the other to attain a higher maximum heat flux and then

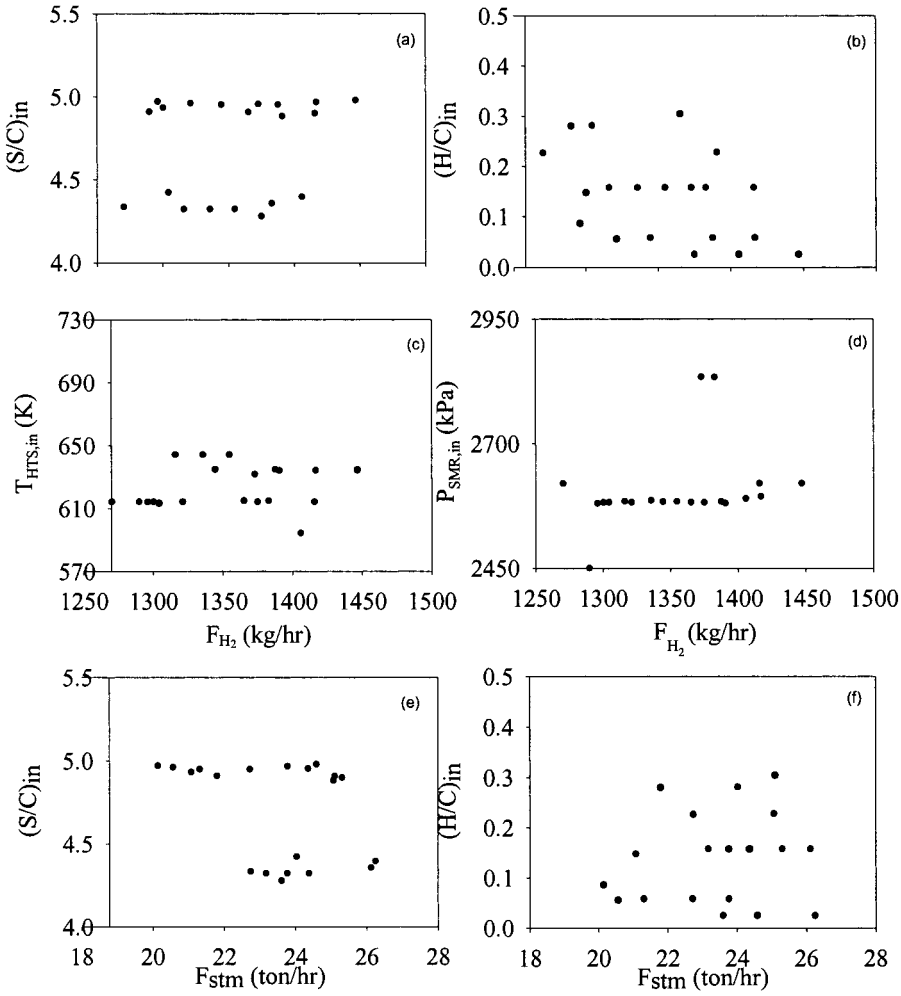

Figure 7. Decision variables for the Pareto set of Figure 6 for three objectives. $(H/C)_{in}$ and $(S/C)_{in}$ are plotted against F_{H_2} in parts a and b and against F_{stm} in parts e and f. Optimal T_{SMR} obtained was the same for all chromosomes and is equal to 801 K.

diminishes slightly more slowly to maintain a higher heat flux at the tube exit. In this way, more furnace heat duty is supplied to drive the forward reforming reactions, leading to a higher conversion and producing more hydrogen. At the same time, more heat is available for recovery at the tube exit for steam generation. Although chromosome 12 involves higher hydrogen and steam production as compared to chromosome 7 (Table 3), it cannot be said to be superior to the latter because higher production comes at the expense of higher reformer heat duty, Q_{SR}, the third objective which was minimized. In other words, for the same $(S/C)_{in}$ and $(H/C)_{in}$, higher hydrogen and steam production are possible provided Q_{SR} is also higher. This explains the scatter in $(S/C)_{in}$ and $(H/C)_{in}$ with respect to F_{H_2} and F_{stm} when Q_{SR} is optimized, as in the case of triple-objective optimization (Figure 7).

As mentioned, we can only compare the results of optimization with the industrial operating case 1 (Table 2) meaningfully provided that the reformer heat duties, Q_{SR}, involved in both are similar. The reformer heat duty associated with industrial operation is very similar to that of chromosome 17 (Table 3). Thus, for a similar duty, the optimal solution of chromosome 17 provides approximately 4% more hydrogen production and 1% more steam generation when compared to industrial operation. Therefore, some improvement can be achieved by operating the industrial hydrogen plant under the conditions predicted by multiobjective optimization. The choice of the "best" operating point in the Pareto set will depend on cost considerations or other subjective criteria based on engineers' experience.

Conclusions

An existing steam reformer based on a refinery off-gas feed is simulated using a rigorous model, which accounts for the hydrogenolysis of heavier hydrocarbons into methane. The model is able to predict the industrial operating data. Subsequently, multiobjective optimization of the complete hydrogen plant using off-gas as the feed is successfully performed. Differences are found between the optimal heat flux profiles obtained for this and for the methane case. Consequently, instantaneous methanation of higher hydrocarbons cannot be an acceptable assumption if we desire to predict the optimal reformer axial heat flux profile. The optimization results show that there exists good scope for improvement in the current operation of the industrial unit studied.

Acknowledgment

The authors thank B. S. Mohanakkannan and J. K. Rajesh for several discussions and for providing practical insights on hydrogen plant operation.

Appendix I. Complete Set of Equations for the Steam Reformer Model

(a) Kinetic Model

$$\frac{dx_i}{dl} = \left(\frac{\pi d_i^2}{4}\right)\frac{R\rho_b\eta_i r_i}{F}; \quad x_i = 0 \text{ at } l = 0,\ x_i = 1, 2, ..., 6 \tag{A1}$$

$$\frac{dP}{dl} = -\frac{1.75G^2(1-\epsilon_b)}{\phi_s D_p \epsilon_b^3 \rho_g}; \quad P = P_{in} \text{ at } l = 0 \tag{A2}$$

$$r_1 = \frac{k_1 y_{C_2H_6}}{P^{1.4} y_{H_2}^{2.4}}$$

$$\text{where } k_1 = 5.18 \times 10^{14} \exp\left(\frac{-2.04 \times 10^4}{T}\right) \tag{A3}$$

$$r_2 = \frac{k_2 y_{C_3H_8}}{P^2 y_{H_2}^3}$$

$$\text{where } k_2 = 1.95 \times 10^{14}\beta_2 \exp\left(\frac{-3.22 \times 10^4}{T}\right); \quad \beta_2 = 1.9 \times 10^7 \tag{A4}$$

$$r_3 = \frac{k_3 y_{C_4H_{10}}}{P^{0.59} y_{H_2}^{1.59}}$$

$$\text{where } k_3 = 3.33 \times 10^{20}\beta_3 \exp\left(\frac{-2.86 \times 10^4}{T}\right); \quad \beta_3 = 10^{-4} \tag{A5}$$

$$r_4 = \frac{k_4}{E^2 y_{H_2}^{2.5}\sqrt{P}}\left(y_{CH_4} y_{H_2O} - \frac{P^2 y_{H_2}^3 y_{CO}}{K_4}\right) \tag{A6}$$

$$r_5 = \frac{k_5 P}{E^2 y_{H_2}}\left(y_{CO} y_{H_2O} - \frac{y_{H_2} y_{CO_2}}{K_5}\right) \tag{A7}$$

$$r_6 = \frac{k_6}{E^2 y_{H_2}^{3.5}\sqrt{P}}\left(y_{CH_4} y_{H_2O}^2 - \frac{y_{H_2}^4 y_{CO_2}}{K_4 K_5}\right) \tag{A8}$$

$$E = \left[1 + P(K_{CO} y_{CO} + K_{CH_4} y_{CH_4} + K_{H_2} y_{H_2}) + K_{H_2O}\frac{y_{H_2O}}{y_{H_2}}\right] \tag{A9}$$

$$r = z_{CH_4,in} + 2z_{C_2H_6,in} + 3z_{C_3H_8,in} + 4z_{C_4H_{10},in} \tag{A10}$$

$$F = F_{HC,in} R$$

$$\text{where } R = 1 + r[(S/C)_{in} + (H/C)_{in} + (M/C)_{in} + (D/C)_{in}] \tag{A11}$$

$$y_{C_2H_6} = \frac{z_{C_2H_6,in} - x_1}{R + 2(x_4 + x_6)} \tag{A12}$$

$$y_{C_3H_8} = \frac{z_{C_3H_8,in} - x_2}{R + 2(x_4 + x_6)} \tag{A13}$$

$$y_{C_4H_{10}} = \frac{z_{C_4H_{10},in} - x_3}{R + 2(x_4 + x_6)} \tag{A14}$$

$$y_{CH_4} = \frac{z_{CH_4,in} + 2x_1 + 3x_2 + 4x_3 - x_4 - x_6}{R + 2(x_4 + x_6)} \tag{A15}$$

$$y_{H_2O} = \frac{r(S/C)_{in} - x_4 - x_5 - 2x_6}{R + 2(x_4 + x_6)} \tag{A16}$$

$$y_{CO} = \frac{r(M/C)_{in} + x_4 - x_5}{R + 2(x_4 + x_6)} \tag{A17}$$

$$y_{CO_2} = \frac{r(D/C)_{in} + x_5 + x_6}{R + 2(x_4 + x_6)} \tag{A18}$$

$$y_{H_2} = \frac{r(H/C)_{in} - x_1 - 2x_2 - 3x_3 + 3x_4 + x_5 + 4x_6}{R + 2(x_4 + x_6)} \tag{A19}$$

(b) Energy Balance

$$\frac{dT}{dl} = \frac{1}{GC_p}\left\{\frac{4q}{d_i} + \rho_b\sum_{i=1}^{6}(-\Delta H_i)\eta_i r_i\right\}; \quad T = T_{in} \text{ at } l = 0 \tag{A20}$$

The inner wall temperature of the tube, $T_{w,i}$, is obtained by equating q to the heat flux due to convective heat transfer to the gas mixture and catalyst bed from the inner surface of the tubes:

$$q = h_{in}(T_{w,i} - T) \tag{A21}$$

$$h_{in} = 0.4\frac{K_g}{D_p}\left\{2.58\left(\frac{D_p G}{\mu}\right)^{1/3}\left(\frac{C_p\mu}{K_g}\right)^{1/3} + 0.094\left(\frac{D_p G}{\mu}\right)^{0.8}\left(\frac{C_p\mu}{K_g}\right)^{0.4}\right\} \tag{A22}$$

The outer wall temperature of the tube, $T_{w,o}$, is obtained from the following relation:

$$T_{w,o} = T_{w,i} + \frac{q}{2K_w}\ln\left(\frac{d_o}{d_i}\right) \tag{A23}$$

(c) Diffusion Model

$$\eta_k = \frac{\int_{v=0}^{v=\alpha} r_k(\bar{y}_{i,n}, T, P)\, dv}{r_k(y_{i,n}, T, P)\, l_c} \qquad k = 1, 2, ..., 6 \tag{A24}$$

where $\bar{y}_{i,n}$ represents the mole fraction of component i

at the nth collocation point inside the catalyst pellet and l_c represents the characteristic length of the catalyst pellet. The $\bar{y}_{i,n}$ values are obtained by solving the following coupled set of $8M$ equations: $3M$ algebraic and $5M$ differential equations (which are transformed into algebraic equations by OCFE):

$$\frac{d^2\bar{y}_{C_2H_6,n}}{dv^2} = a^2 l_c^2 \left\{\frac{\rho_s(r_4 + r_5 + 2r_6)_b}{(P/RT)D^e_{C_2H_6}}\right\}\frac{r_{1,n}}{r_{H_2O,1}} \qquad n = 2, 3, ..., M+1 \quad \text{(A25)}$$

$$\frac{d^2\bar{y}_{C_3H_8,n}}{dv^2} = a^2 l_c^2 \left\{\frac{\rho_s(r_4 + r_5 + 2r_6)_b}{(P/RT)D^e_{C_3H_8}}\right\}\frac{r_{2,n}}{r_{H_2O,1}} \qquad n = 2, 3, ..., M+1 \quad \text{(A26)}$$

$$\frac{d^2\bar{y}_{C_4H_{10},n}}{dv^2} = a^2 l_c^2 \left\{\frac{\rho_s(r_4 + r_5 + 2r_6)_b}{(P/RT)D^e_{C_4H_{10}}}\right\}\frac{r_{3,n}}{r_{H_2O,1}} \qquad n = 2, 3, ..., M+1 \quad \text{(A27)}$$

$$\frac{d^2\bar{y}_{CH_4,n}}{dv^2} = a^2 l_c^2 \left\{\frac{\rho_s(r_4 + r_5 + 2r_6)_b}{(P/RT)D^e_{CH_4}}\right\}\frac{(-2r_{1,n} - 3r_{2,n} - 4r_{3,n} + r_{4,n} + r_{6,n})}{r_{H_2O,1}} \qquad n = 2, 3, ..., M+1 \quad \text{(A28)}$$

$$\frac{d^2\bar{y}_{H_2O,n}}{dv^2} = a^2 l_c^2 \left\{\frac{\rho_s(r_4 + r_5 + 2r_6)_b}{(P/RT)D^e_{H_2O}}\right\}\frac{(r_{4,n} + r_{5,n} + 2r_{6,n})}{r_{H_2O,1}} \qquad n = 2, 3, ..., M+1 \quad \text{(A29)}$$

$$\bar{y}_{CO,n} = y_{CO} - \frac{1}{D^e_{CO}}[4D^e_{C_2H_6}(\bar{y}_{C_2H_6,n} - y_{C_2H_6}) + 6D^e_{C_3H_8}(\bar{y}_{C_3H_8,n} - y_{C_3H_8}) + 8D^e_{C_4H_{10}}(\bar{y}_{C_4H_{10},n} - y_{C_4H_{10}}) + 2D^e_{CH_4}(\bar{y}_{CH_4,n} - y_{CH_4}) - D^e_{H_2O}(\bar{y}_{H_2O,n} - y_{H_2O})] \qquad n = 2, 3, ..., M+1 \quad \text{(A30)}$$

$$\bar{y}_{CO_2,n} = y_{CO_2} - \frac{1}{D^e_{CO_2}}[2D^e_{C_2H_6}(\bar{y}_{C_2H_6,n} - y_{C_2H_6}) + 3D^e_{C_3H_8}(\bar{y}_{C_3H_8,n} - y_{C_3H_8}) + 4D^e_{C_4H_{10}}(\bar{y}_{C_4H_{10},n} - y_{C_4H_{10}}) + D^e_{CH_4}(\bar{y}_{CH_4,n} - y_{CH_4}) - D^e_{H_2O}(\bar{y}_{H_2O,n} - y_{H_2O})] \qquad n = 2, 3, ..., M+1 \quad \text{(A31)}$$

$$\bar{y}_{H_2O,n} = 1 - (\bar{y}_{C_2H_6} + \bar{y}_{C_3H_8} + \bar{y}_{C_4H_{10}} + \bar{y}_{CH_4} + \bar{y}_{H_2O} + \bar{y}_{CO} + \bar{y}_{CO_2}) \qquad n = 2, 3, ..., M+1 \quad \text{(A32)}$$

Boundary conditions:

$$\bar{y}_{i,1} = y_i \qquad i = C_2H_6, C_3H_8, C_4H_{10}, CH_4, H_2O, CO, CO_2, H_2 \quad \text{(A33)}$$

$$\frac{d\bar{y}_{i,M+2}}{dv} = 0 \qquad i = C_2H_6, C_3H_8, C_4H_{10}, CH_4, H_2O, CO, CO_2, H_2 \quad \text{(A34)}$$

(d) Data. Correlations for C_p, μ, K_g, and ΔH_i were obtained from Hysys, while those for k_i, K_i ($i = 4-6$), and D^e_i ($i = CH_4$, H_2O, CO, CO_2, H_2) were taken from Elnashaie and Elshishini.[6] K_j ($j = C_2H_6$, C_3H_8, C_4H_{10}) were assumed to be identical to K_{CH_4}. Correlations for k_1, k_2, and k_3 were obtained from Sinfelt et al.,[12] Burke and Ko,[13] and Orlickas et al.,[14] respectively. The gas mixture was assumed to be ideal for computing ρ_g. The average molecular weight and molar flow rate at the reformer inlet were used to compute G.

Nomenclature

a = fraction of half catalyst pellet thickness in which the concentrations change
$A-E$ = coefficients in eq 13
C_p = specific heat of the process gas (kcal/kmol/K)
d_i, d_o = internal/external diameter of the reformer tube (m)
D^e_i = effective diffusivity of component i in the catalyst (m^2/h)
D_p = equivalent diameter of the catalyst pellet (Raschig ring) (m)
$(D/C)_{in}$ = carbon dioxide to carbon molar ratio in the feed
F = total molar feed rate (kmol/h)
F_{H_2}, F_{stm} = mass flow rate of hydrogen/export steam from the unit (kg or ton/h)
$F_{HC,in}$ = molar flow rate of hydrocarbons to the reformer (kmol/h)
G = mass velocity of the process gas (kg/h/m^2)
h_{in} = heat-transfer coefficient inside the tube (kcal/h/m^2/K)
$(H/C)_{in}$ = recycle hydrogen to carbon molar ratio in the feed
k_1-k_6 = rate constants of reactions 1−6
K_g, K_w = thermal conductivity of the process gas/tube wall (kcal/h/m/K)
K_4, K_5 = equilibrium rate constants of reactions 4 and 5
K_i = equilibrium adsorption constants for component i (kPa^{-1})
l_c = characteristic length of the catalyst pellet (m)
L = length of the reformer tube (m)
M = number of internal collocation points
$(M/C)_{in}$ = carbon monoxide to carbon molar ratio in the feed
P = pressure in the reformer tube (kPa)
$P_{SR,in}$ = pressure at the inlet to the steam reformer (kPa)
q = heat flux on the reformer tubes (kcal/h/m^2)
Q = heat duty (Gcal/h)
Q_{SR} = heat duty required by the steam reformer (Gcal/h)
Q_{fuel} = heat duty supplied by external fuel (Gcal/h)
r_i = rate of reaction i at the catalyst surface (kmol/kg of catalyst/h)
$r_{i,n}$ = rate of reaction i at the nth collocation point in the catalyst pellet (kmol/kg of catalyst/h)
$(S/C)_{in}$ = steam to carbon molar ratio in the feed
T = process gas temperature (K)
T_g = temperature of the furnace gas (K)
$T_{SR,in}$, $T_{HTS,in}$ = temperature at the inlet to the reformer/HT shift converter (K)
$T_{w,i}$, $T_{w,o}$ = inner/outer wall temperature of the tube (K)
v = dimensionless distance within the half thickness of the catalyst pellet ($v = 0$ at the catalyst surface)
x_i, x_j = conversion of reaction i ($i = 1-6$) or conversion of component j ($j = C_2H_6$, C_3H_8, C_4H_{10}, CH_4, H_2O), based on the hydrocarbon feed

$\underline{y_i}$ = mole fraction of the component i in the bulk gas
$y_{i,n}$ = mole fraction of component i at the nth collocation point inside the catalyst pellet
z = axial location in the reformer tube (m)
z^* = axial location in the reformer tube where the maximum heat flux occurs (m)
z_i = mole fraction of component i in the hydrocarbon feed, $i = CH_4, C_2H_6, C_3H_8, C_4H_{10}$

Greek Symbols

β_2, β_3 = multiplication factor for the forward rate constants of reactions 2 and 3
ϵ_b = void fraction of the catalyst bed
ϵ_c = porosity of the catalyst pellet
ϕ_s = sphericity of the catalyst pellet
η_i = effectiveness factor for reaction i
η_{CH_4}, η_{CO_2} = effectiveness factors for conversion of CH_4 and CO_2
μ = viscosity of the gas mixture (kg/m/h)
ρ_b = bulk density of the catalyst (kg/m^3)
ρ_g = density of the gas mixture (kg/m^3)
ρ_s = catalyst density (kg/m^3)
τ = tortuosity of the catalyst pellet
$(-\Delta H_r)_i$ = heat of the ith reaction (kcal/kmol)

Subscripts

E1 = steam generator
E2 = preheater for boiler feedwater
HC = hydrocarbon
HTS = HT shift converter
SR = steam reformer

Literature Cited

(1) Oh, P. P.; Ray, A. K.; Rangaiah, G. P. Triple-Objective Optimization of an Industrial Hydrogen Plant. *J. Chem. Eng. Jpn.* **2001**, *34* (11), 1341.

(2) Rostrup-Nielsen, J. R.; Tottrup, P. B. Steam Reforming of Heavy Feedstocks. *Proc. Symp. Sci. Catal. Appl. Ind.* **1979**, 379.

(3) Hyman, M. H. Simulate Methane Reformer Reactions. *Hydrocarbon Process.* **1968**, *47*, 131.

(4) Singh, C. P. P.; Saraf, D. N. Simulation of Side Fired Steam-Hydrocarbon Reformers. *Ind. Eng. Chem. Process Des. Dev.* **1979**, *16*, 313.

(5) Alatiqi, L. M.; Meziou, A. M.; Gasmelseed, G. A. Modeling, Simulation and Sensitivity Analysis of Steam-Methane Reformers. *Int. J. Hydrogen Energy* **1989**, *14*, 241.

(6) Elnashaie, S. S. E. H.; Elshishini, S. S. *Modelling, Simulation and Optimization of Industrial Catalytic Fixed-Bed Reactors*; Gordon and Breach: Amsterdam, The Netherlands, 1993.

(7) Rajesh, J. K.; Gupta, S. K.; Rangaiah, G. P.; Ray, A. K. Multiobjective optimization of Steam Reformer Performance using Genetic Algorithm. *Ind. Eng. Chem. Res.* **2000**, *39*, 706.

(8) Rajesh, J. K.; Gupta, S. K.; Rangaiah, G. P.; Ray, A. K. Multiobjective optimization of Industrial Hydrogen Plants. *Chem. Eng. Sci.* **2001**, *56*, 999.

(9) Xu, J.; Froment, G. F. Methane Steam Reforming, Methanation and Water-Gas Shift: I. Intrinsic Kinetics. *Am. Inst. Chem. Eng. J.* **1989**, *35*, 88.

(10) Elnashaie, S. S. E. H.; Alhabdan, F. M. Mathematical Modelling and Computer Simulation of Industrial Water−Gas Shift Converters. *Math. Comput. Model.* **1989**, *12*, 1017.

(11) Chlendi, M.; Tondeur, D.; Rolland, F. Method to Obtain a Compact Representation of Process Performances from a Numerical Simulator: Example of Pressure Swing Adsorption for Pure Hydrogen Production. *Gas Sep. Purif.* **1995**, *9*, 125.

(12) Sinfelt, J. H.; Taylor, W. F.; Yates, D. J. C. Catalysis over Supported Metals. III. Comparison of Metals of Known Surface Area for Ethane Hydrogenolysis. *J. Phys. Chem.* **1965**, *69*, 95.

(13) Burke, P. A.; Ko, E. I. Propane Hydrogenolysis over Supported Nickel Catalysts: Structural and Support Effects. *J. Catal.* **1989**, *116*, 230.

(14) Orlickas, A.; Hoffman, T. W.; Shaw, I. D.; Reilly, P. M. The Hydrogenolysis of *n*-Butane on a Nickel on Silica Catalyst: I. A Kinetic Model. *Can. J. Chem. Eng.* **1972**, *50*, 628.

(15) Rostrup-Nielsen, J. R. Catalytic Steam Reforming. In *Catalysis*: *Science and Technology*; Anderson, A. R., Boudart, M., Eds.; Springer: Berlin, 1984; Vol. 5.

(16) King, D. L., Bochow, C. E., Jr. What should an owner/operator know when choosing an SMR/PSA plant? *Hydrocarbon Process.* **2000**, *79*, 39.

(17) Srinivas, N.; Deb, K. Multiobjective function optimization using nondominated sorting genetic algorithms. *Evol. Comput.* **1995**, *2*, 221.

(18) Bhaskar, V.; Gupta, S. K.; Ray, A. K. Applications of multiobjective optimization in chemical engineering. *Rev. Chem. Eng.* **2000**, *16*, 1.

(19) Plehiers, P. M.; Froment, G. F. Coupled Simulation of Heat Transfer and Reaction in a Steam Reforming Furnace. *Chem. Eng. Technol.* **1989**, *12*, 20.

Received for review March 26, 2001
Revised manuscript received October 2, 2001
Accepted February 4, 2002

IE010277N